



Title	Multiple-shocks induced nanocrystallization in iron
Author(s)	Matsuda, Tomoki; Sano, Tomokazu; Arakawa, Kazuto et al.
Citation	Applied Physics Letters. 2014, 105(2), p. 021902
Version Type	VoR
URL	https://hdl.handle.net/11094/89438
rights	This article may be downloaded for personal use only. Any other use requires prior permission of the author and AIP Publishing. This article appeared in Matsuda T., Sano T., Arakawa K., et al. Multiple-shocks induced nanocrystallization in iron. Applied Physics Letters, 105(2), 021902 and may be found at https://doi.org/10.1063/1.4890389 .
Note	

The University of Osaka Institutional Knowledge Archive : OUKA

<https://ir.library.osaka-u.ac.jp/>

The University of Osaka

Multiple-shocks induced nanocrystallization in iron

Cite as: Appl. Phys. Lett. **105**, 021902 (2014); <https://doi.org/10.1063/1.4890389>

Submitted: 13 April 2014 • Accepted: 04 July 2014 • Published Online: 14 July 2014

Tomoki Matsuda (松田朋己), Tomokazu Sano (佐野智一), Kazuto Arakawa (荒河一渡), et al.



View Online



Export Citation



CrossMark

ARTICLES YOU MAY BE INTERESTED IN

[Dislocation structure produced by an ultrashort shock pulse](#)

Journal of Applied Physics **116**, 183506 (2014); <https://doi.org/10.1063/1.4901928>

[Femtosecond laser peening of 2024 aluminum alloy without a sacrificial overlay under atmospheric conditions](#)

Journal of Laser Applications **29**, 012005 (2017); <https://doi.org/10.2351/1.4967013>

[Femtosecond laser quenching of the \$\epsilon\$ phase of iron](#)

Applied Physics Letters **83**, 3498 (2003); <https://doi.org/10.1063/1.1623935>

Trailblazers. New

Meet the Lock-in Amplifiers that measure microwaves.

Zurich Instruments [Find out more](#)

Multiple-shocks induced nanocrystallization in iron

Tomoki Matsuda (松田朋己),¹ Tomokazu Sano (佐野智一),^{1,2} Kazuto Arakawa (荒河一渡),^{2,3} and Akio Hirose (廣瀬明夫)¹

¹*Division of Materials and Manufacturing Science, Graduate School of Engineering, Osaka University, Suita, Osaka 565-0871, Japan*

²*JST, CREST, Suita, Osaka 565-0871, Japan*

³*Department of Material Science, Interdisciplinary Faculty of Science and Engineering, Shimane University, Matsue, Shimane 690-8504, Japan*

(Received 13 April 2014; accepted 4 July 2014; published online 14 July 2014)

We found that multiple shots of femtosecond laser-driven shock pulses changed coarse crystalline iron grains with a size of $140\ \mu\text{m}$ into nanocrystals with a high density of dislocations, which had never been observed in conventional shock processes. We performed metallurgical microstructure observations using transmission electron microscopy (TEM) and hardness measurements using nanoindentation on cross-sections of shocked iron. TEM images showed that grains with sizes from $10\ \text{nm}$ through $1\ \mu\text{m}$ exist within $2\ \mu\text{m}$ of the surface, where the dislocation density reached $2 \times 10^{15}\ \text{m}^{-2}$. Results of the hardness measurements showed a significant increase in hardness in the nanocrystallized region. We suggest that the formation of a high density of dislocations, which is produced by a single shock, induces local three-dimensional pile-up by the multiple-shocks, which causes grain refinement at the nanoscale. © 2014 AIP Publishing LLC.

[<http://dx.doi.org/10.1063/1.4890389>]

Nanocrystallization is one of the most important methods for strengthening materials.¹ It is associated with grain refinement and is generally explained by the Hall-Petch law where flow stress increases with a decrease in the grain size. Plastic deformation processes, such as accumulative roll bonding,² equal-channel angular pressing,³ and high pressure torsion,^{4,5} are utilized for nanocrystallization, where formation of dislocations is a dominant factor. Nanocrystalline grains are formed with increasing strain by the following mechanism;⁵ (i) dislocation accumulation occurs, (ii) subgrain boundaries form, (iii) some dislocations are annihilated at subgrain boundaries to increase the misorientation angles, (iv) balance is established between generation of dislocations and absorption of dislocations at grain boundaries. Thus, the inside of each nanograin has a low density of dislocations.

Shock compression induces plastic deformation associated with dislocation slip or twinning at high-strain-rate.^{6–10} A high density of dislocations is formed during the shock compression because dislocation generation is more effective for high-strain-rate deformation, as expressed by Orowan equation,¹¹ where the strain rate is composed of two terms of the dislocation velocity and the generation rate of dislocations. The process of formation of dislocations in shock compression has been discussed based on several models^{7,8,12,13} and simulations,^{14–16} which suggest that high density of dislocations are produced from a combination of generation in the shock front and multiplication behind it. Eventually, the microstructure consists of dislocation substructures, such as microbands or cells, which are formed depending on the pressure and duration of the shock pulse.^{7,8} Shock-induced nanocrystallization, however, has not been achieved in a single shock pulse in spite of the formation of a high density of dislocations.

Femtosecond laser-driven shock compression, in particular, features a short duration pulse,^{17–21} which restrain the

shock-induced secondary effects, such as a temperature rise accompanied by an increase in entropy in shock compression. Thus, femtosecond laser-driven shock compression induces a higher density of dislocations in the material near the surface compared to the conventional shock compression.^{22,23} Since a high density of dislocations are formed in the grains after a single shock pulse, we can predict that additional shock pulses will induce interactions between pre-existing and newly generated dislocations, which would lead to their multiplication and an increase of misorientation from the pre-shocked state due to the accumulation of dislocations. The additional shock pulses will also play an important role in retaining dislocations inside the grains, in contrast to conventional plastic deformation processes,⁵ which has the potential to lead to a higher strengthening effect.

However, the microstructure after multiple-shock compressions has not been clarified. The purpose of this study is to achieve nanocrystallization in iron, with a high density of dislocations inside the nanograins, by using multiple shots of femtosecond laser-driven shock pulses. We performed metallurgical microstructure observation and hardness measurement to confirm the presence of nanocrystallization and to clarify the relation between the grain refinement and the distribution of dislocations.

Polycrystalline pure iron with purity of 99.99% was used as a specimen. The average grain size was $140\ \mu\text{m}$ after annealing at $1123\ \text{K}$ to recover from the initial strain and for grain coarsening. Femtosecond laser (Spitfire; Spectra-Physics Inc.) pulses with a wavelength of $800\ \text{nm}$, a pulse duration of $130\ \text{fs}$ at full width at half maximum, and a pulse energy of $0.20\ \text{mJ}$ were focused on the mirror finished surface with a spot diameter of $50\ \mu\text{m}$. A schematic illustration of the experimental procedure is shown in Fig. 1. Laser pulses were irradiated left-to-right along the x direction at an interval of $8\ \mu\text{m}$ at a steady rate, and the scan direction was

reversed. The one-axis scanning was repeated along the y direction at $8\text{ }\mu\text{m}$ intervals, which results in overlapping multiple-shocks in two dimensions (Fig. 1(a)). A focused Ga^+ ion beam (30 kV) instrument equipped with a micro-sampling system was used to prepare cross-sectional transmission electron microscopy (TEM) (JEM-2010; JEOL) specimens (Fig. 1(b)). The surface of the specimen was coated with gold and tungsten before fabrication in order to prevent irradiation damage by the ion beam which is likely to induce prismatic dislocation loops. The cross-section parallel to the shock direction was observed with 200 kV electrons. Hardness measurements were performed on the cross-section using nanoindentation (ENT-1100a; ELIONIX) technique (Fig. 1(c)). Prior to the hardness measurements, the cross-sectioned sample was polished by Ar^+ ion beam (5 kV). The applied load was $200\text{ }\mu\text{N}$. The load, holding, and release times were 10, 1, and 10 s, respectively.

Figures 2(a) and 2(b) show the results of dark field TEM (DF-TEM) observations of a cross-section of the multiple-shocked iron. The electron diffraction pattern shown in the inset of Fig. 2(a) was acquired from selected 700 nm diameter area near the surface and shows diffraction rings which reveal the presence of fine grains. Figure 2(a) shows the DF-TEM image acquired from the (211) diffraction spot shown in the inset of Fig. 2(a). Different grains ranging in size from several tens to hundreds of nm whose orientations differ from the matrix are observed within $2\text{ }\mu\text{m}$ of the surface. The size of the refined grains reaches $1\text{ }\mu\text{m}$, as shown in Fig. 2(b). Furthermore, brightness variations which reveal the presence of local misorientations are visible in individual crystal grains. Since local misorientation attributes to the existence of geometrically necessary dislocations,²⁴ we consider that multiple-shocks induce not only nanocrystallization, but also formation of dislocations inside the nanograins. Here, bright field TEM (BF-TEM) image of a cross-section of single shocked iron is shown in Fig. 2(c). In single shocked iron, grain size is reduced to sub-micrometer at least within $1\text{ }\mu\text{m}$ of the surface and uniform dislocations exist without grain refinement below $1\text{ }\mu\text{m}$.

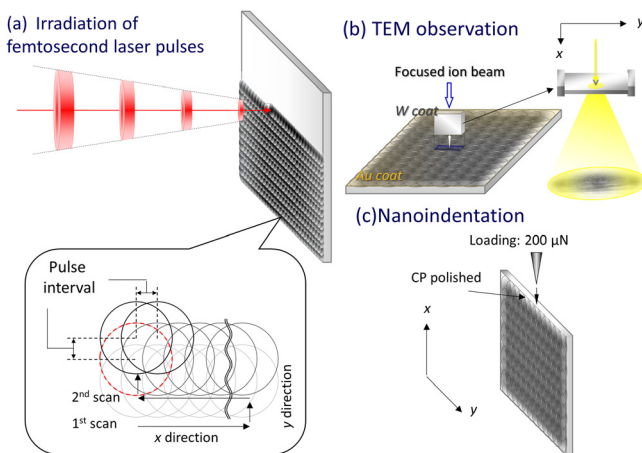


FIG. 1. Schematic illustrations of experimental procedure. (a) Irradiation of femtosecond laser pulses is performed on the mirror finished iron along the x direction and repeated in the perpendicular direction. The microstructure and mechanical property of a cross-section of the multiple-shocked iron are analyzed using (b) TEM and (c) a hardness test using nanoindentation.

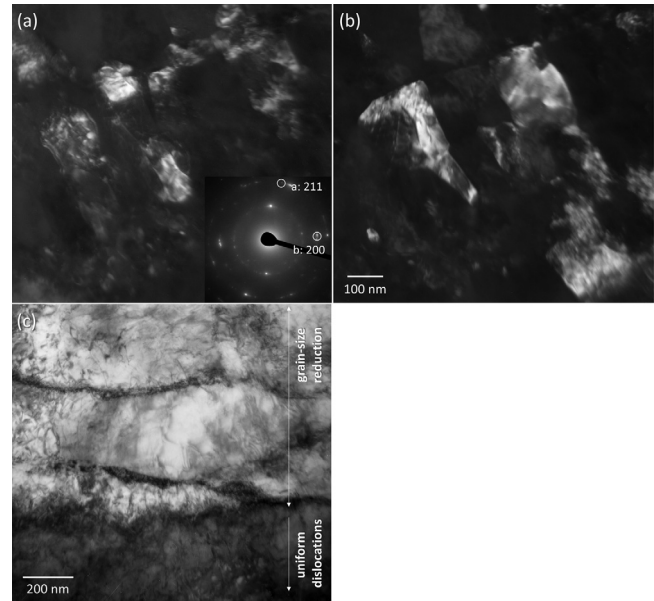


FIG. 2. Grain refinement in iron induced by multiple-shocks and a single shock. (a) DF-TEM image within $1\text{ }\mu\text{m}$ of the surface after multiple-shocks acquired from the 211 spot in the selected 700 nm diameter area electron diffraction pattern. (b) DF-TEM image acquired from the 200 spot in the diffraction. (c) BF-TEM image within $1.5\text{ }\mu\text{m}$ of the surface after a single shock.

BF-TEM images observed at different depth are shown in Figs. 3(a)–3(c). As shown in Fig. 3(a), a high density of dislocations is present inside the refined grains. This fact reveals that local misorientation inside the nanograins observed in DF-TEM images results from the existence of dislocations. A number of dislocation loops and tangles are clearly observed in unrefined grains neighboring nanocrystallized ones, as shown in Fig. 3(b). In contrast, with increasing depth, dislocations become less tangled and more individual, as shown in Fig. 3(c), finally reaching a state that was unaffected by the shocks.

Dislocation loops act as a source to generate more dislocations. Also, tangles result from interactions of dislocations, which indicate multiplication of dislocations. Therefore, a high density of dislocations in unrefined grains that neighbor nanocrystals results from the generation and multiplication of dislocations during the process of multiple-shocks. A higher density of dislocations are formed near the surface in a single shock pulse since a higher pressure is applied. Using multiple-shocks, the increment in dislocations in the upper side is more than that in lower side because of the small secondary effect of the femtosecond laser pulses, which indicates that grain refinement is accompanied by formation of high density of dislocations.

We quantitatively estimate the distribution of dislocations as a function of depth using Ham equation²⁵ expressed by $\rho = 2N/Lt$, where ρ is the dislocation density, N is the number of intersection points between dislocation lines and grid lines drawn on the TEM micrograph, L is the total length of grid lines, and t is the thickness of the TEM sample as shown in Fig. 3(d). The dislocation density in Fig. 3(a), without considering grain boundaries, exceeds $2 \times 10^{15}\text{ m}^{-2}$ which agrees with the value in Fig. 3(b), while it decreases abruptly below $1 \times 10^{15}\text{ m}^{-2}$ below the nanocrystallized

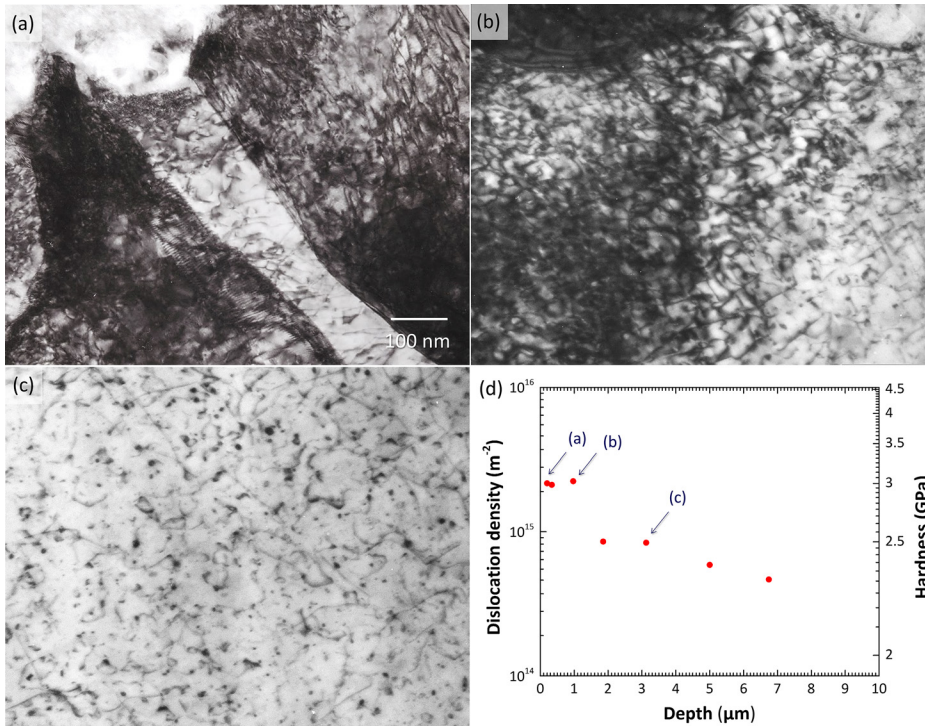


FIG. 3. Bright field TEM images show the existence of dislocations as a function of depth. (a) Coarse grains in a nanocrystallized region within $2\mu\text{m}$ of the surface. (b) An unrefined grain neighboring nanocrystallized ones within $2\mu\text{m}$ of the surface. (c) Low density of dislocations in a deeper region. (d) Distribution of dislocation density with the depth. The right axis shows the hardness corresponding to the dislocation density.

region. In addition, dislocation density in single shocked iron is $6 \times 10^{14} \text{m}^{-2}$ at most in the shallow region where uniform dislocations exist, which is less than that in Fig. 3(c) and steeply decrease with depth.

Figure 4(a) shows the hardness distribution against depth. The hardness increases toward the surface, and it reaches a maximal value of 4.3 GPa at $0.92\mu\text{m}$, which is 2.6 times larger than the matrix hardness of 1.7 GPa. The gradient of the change in hardness against depth is steep within $2.5\mu\text{m}$ of the surface but is gradual in the region deeper than $2.5\mu\text{m}$. The region showing the steep gradient approximately corresponds to that where a high density of dislocations are formed or the nanocrystallized region.

Figure 4(b) shows the load-displacement curves measured at the hardest point and a point in the matrix. The displacement of the hardest point is smaller than that of the matrix at maximal load, and load-displacement curve of the hardest point has no distinct displacement discontinuity, i.e., a pop-in event, which indicates the yielding of the indented metals, while that of the matrix shows multiple pop-in events. Therefore, the curve of the hardest point reveals the increase of the onset stress of plastic flow. This decrease in displacement without pop-in events is also observed in the other hardened points.

We evaluate the effect of dislocations on the hardness using the Bailey-Hirsch relation,²⁶ which is expressed by $\sigma_y = \alpha\mu b\sqrt{\rho}$, where σ_y is the yield strength of the deformed material, α is a constant associated with the dislocation substructure, μ is the shear modulus, b is the magnitude of the Burgers vector, and ρ is the dislocation density. The change in the hardness is $H_y = 3\sigma_y$.²⁷ The hardness values corresponding to the dislocation density are shown in Fig. 3(d) using an α of 0.5, μ of 77.5 GPa, and b of 0.248 nm. We confirm that the estimated hardness approximately corresponds to the measured hardness below the nanocrystallized region. However, the estimated hardness is at most 3.0 GPa within

the nanocrystallized region, which shows that the change in hardness measured cannot be fully accounted for only by the dislocations. Therefore, the steep gradient of the change in hardness is attributed to not only a high density of

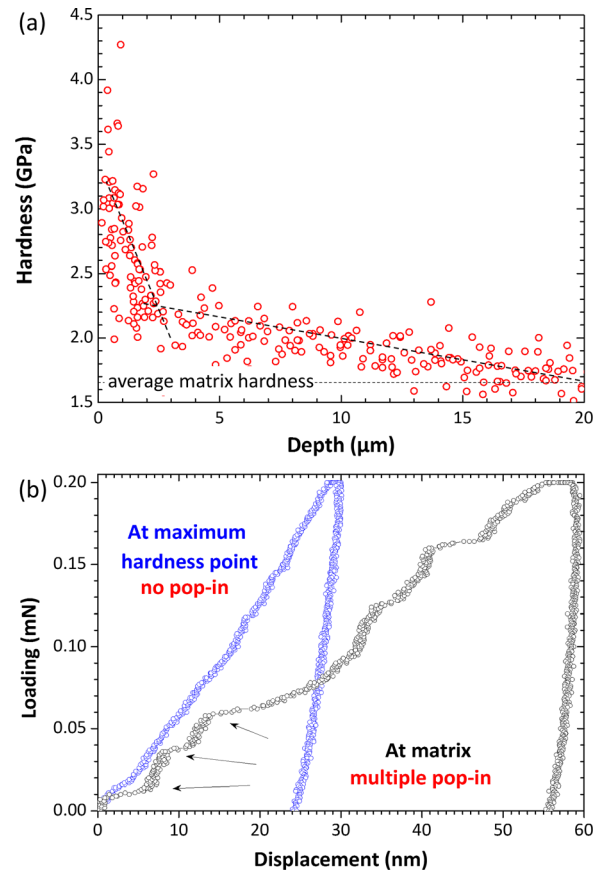


FIG. 4. Results of hardness measurements using nanoindentation. (a) Hardness distribution against depth. (b) Two typical load-displacement curves corresponding to maximum hardness (blue circles) and matrix hardness (black circles).

dislocations, but also grain refinement, which results in creation of nanograins within $2\ \mu\text{m}$ of the surface.

The region where grain size is reduced after a single shock is removed due to multiple shots of laser pulse because laser ablation depth per one pulse exceeds $1.0\ \mu\text{m}$. Therefore, we consider that dislocations formed via a single-shock process, which has steep gradient of the density along shock direction below the grain size-reduced region, just attribute to the formation of eventual microstructure after multiple-shocks. In the case of multiple-shocks along one direction, dislocations would be non-homogeneously piled-up on the slip plane due to their interactions and intersections, which induce the multiplication and result in an increase in dislocation density. In the case of shooting multiple-shocks two-dimensionally on the surface, multiple slips due to an increase in strain promote three dimensional pile-ups of dislocations. As a high-strain-rate deformation induces dislocation generation¹⁰ and formation of a high density of dislocations, the multiple-shocks promote the effective interaction of dislocations and produce such large misorientation as to result in the formation of fine grains. The non-homogeneity of the dislocation structure will induce a wide range of grain size, a prediction that is supported by the results of the TEM observations showing a broad grain size distribution.

In summary, we report the nanocrystallization of iron induced by multiple shots of femtosecond laser-driven shock pulses, which is measured by TEM observations and hardness measurement using nanoindentation. TEM observations show that nanograins with size from 10 nm through $1\ \mu\text{m}$, with a high density of dislocations more than $10^{15}\ \text{m}^{-2}$, are present within $2\ \mu\text{m}$ of the surface, and that comparable dislocations are present in unrefined grain neighboring nanocrystallized ones. Hardness measurement shows the steep gradient of the change in hardness within $2.5\ \mu\text{m}$ of the surface, which approximately corresponds to the nanocrystallized region. Since the change in hardness in the nanocrystallized region cannot be fully accounted for by dislocations, the steep increase of the hardness change is attributed to the combination of grain refinement at the nanoscale and a high density of dislocations in the grains. From the distribution of refined grains and dislocations, we suggest that grain refinement is due to a local three-dimensional pile-up of a high density of dislocation,

which is produced by a single shock, by the multiple-shocks.

This work was supported in part by JSPS KAKENHI Grant Nos. 22224012 and 25420778.

- ¹R. Valiev, *Nature Mater.* **3**, 511 (2004).
- ²Y. Saito, H. Utsunomiya, N. Tsuji, and T. Sakai, *Acta Mater.* **47**, 579 (1999).
- ³V. M. Segal, *Mater. Sci. Eng. A* **197**, 157 (1995).
- ⁴P. W. Bridgeman, *Studies in Large Plastic Flow and Fracture* (McGraw-Hill, New York, 1952).
- ⁵Y. Ito and Z. Horita, *Mater. Sci. Eng. A* **503**, 32 (2009).
- ⁶J. W. Swegle and D. E. Grady, *J. Appl. Phys.* **58**, 692 (1985).
- ⁷M. A. Meyers, F. Gregori, B. K. Kad, M. S. Schneider, D. H. Kalantar, B. A. Remington, G. Ravichandran, T. Boehly, and J. S. Wark, *Acta Mater.* **51**, 1211 (2003).
- ⁸C. H. Lu, B. A. Remington, B. R. Maddox, B. Kad, H. S. Park, S. T. Prishbrey, and M. A. Meyers, *Acta Mater.* **60**, 6601 (2012).
- ⁹A. Higginbotham, M. J. Suggit, E. M. Bringa, P. Erhart, J. A. Hawrelak, G. Mogni, N. Park, B. A. Remington, and J. S. Wark, *Phys. Rev. B* **88**, 104105 (2013).
- ¹⁰S. J. Wang, M. L. Sui, Y. T. Chen, Q. H. Lu, E. Ma, X. Y. Pei, Q. Z. Li, and H. B. Hu, *Sci. Rep.* **3**, 1086 (2013).
- ¹¹E. Orowan, *Proc. Phys. Soc. London* **52**, 8 (1940).
- ¹²C. S. Smith, *Trans. AIME* **212**, 574 (1958).
- ¹³E. Hornbogen, *Acta Metall.* **10**, 978 (1962).
- ¹⁴B. L. Holian and P. S. Lomdahl, *Science* **280**, 2085 (1998).
- ¹⁵M. A. Shehadeh, E. M. Bringa, H. M. Zbib, J. M. McNaney, and B. A. Remington, *Appl. Phys. Lett.* **89**, 171918 (2006).
- ¹⁶E. M. Bringa, K. Rosolankova, R. E. Rudd, B. A. Remington, J. S. Wark, M. Duchaineau, D. H. Kalantar, J. Hawrelak, and J. Belak, *Nature Mater.* **5**, 805 (2006).
- ¹⁷R. Evans, A. D. Badger, F. Fallies, M. Mahdih, and T. A. Hall, *Phys. Rev. Lett.* **77**, 3359 (1996).
- ¹⁸K. T. Gahagan, D. S. Moore, D. J. Funk, R. L. Rabie, and S. J. Buelow, *Phys. Rev. Lett.* **85**, 3205 (2000).
- ¹⁹S. D. McGrane, D. S. Moore, D. J. Funk, and R. L. Rabie, *Appl. Phys. Lett.* **80**, 3919 (2002).
- ²⁰B. J. Demaske, V. V. Zhakhovsky, N. A. Inogamov, and I. I. Oleynik, *Phys. Rev. B* **87**, 054109 (2013).
- ²¹J. P. Cuq-Lelandais, M. Boustie, L. Berthe, T. de Rességuier, P. Combis, J. P. Colombier, M. Nivard, and A. Claverie, *J. Phys. D Appl. Phys.* **42**, 065402 (2009).
- ²²M. Tsujino, T. Sano, T. Ogura, M. Okoshi, N. Inoue, N. Ozaki, R. Kodama, K. F. Kobayashi, and A. Hirose, *Appl. Phys. Express* **5**, 022703 (2012).
- ²³T. Sano, H. Mori, E. Ohmura, and I. Miyamoto, *Appl. Phys. Lett.* **83**, 3498 (2003).
- ²⁴M. F. Ashby, *Philos. Mag.* **21**, 399 (1970).
- ²⁵R. K. Ham, *Philos. Mag.* **6**, 1183 (1961).
- ²⁶J. E. Bailey and P. B. Hirsch, *Philos. Mag.* **5**, 485 (1960).
- ²⁷A. Belyakov, Y. Sakai, T. Hara, Y. Kimura, and K. Tsuzaki, *Metall. Mater. Trans. A* **32**, 1769 (2001).